Applied Mathematical Sciences, Vol. 3, 2009, no. 17, 825 - 837

Numerical Computation of the Eigenstructure of Cylindrical Acoustic Waveguides with Heated (or Cooled) Walls

Brian J. McCartin

Applied Mathematics, Kettering University
1700 West University Avenue, Flint, MI 48504-4898, USA
bmccarti@kettering.edu

Abstract

A perturbation procedure for the modes and cut-off frequencies of cylindrical acoustic waveguides of arbitrary cross-section with a small temperature gradient along the walls was presented in [1, 2]. In the present paper, that work is extended to arbitrary wall temperature distributions ("warm waveguides") as outlined in [3]. We utilize a physical formulation due to DeSanto [4] which incorporates both an inhomogeneous sound speed and a density gradient. This physical model is altered to include an axial velocity component [5]. The associated eigenvalue problem [6] is then discretized via the Control Region Approximation [7, 8] which is a finite difference procedure applicable on arbitrary computational grids [9]. The resulting sparse generalized matrix eigenvalue problem [10] is then solved numerically [11] using MATLAB©. This general computational procedure is then used to study the acoustical effect of heating (or cooling) the walls of rectangular waveguides [12].

Mathematics Subject Classification: 35P99, 35Q99, 65F15, 65M06, 76M20, 76Q05, 80A20, 80M20

Keywords: acoustic waveguides, temperature gradient, Control Region Approximation, generalized eigenvalue problem, inhomogeneous waveguide

1 Introduction

Modal propagation characteristics of cylindrical acoustic waveguides at constant temperature have been investigated analytically for canonical duct cross-sections such as rectangular and circular [6] and numerically for general simply-connected cross-sections [7]. However, if there is a temperature variation across

the duct, then these analyses are inadequate. This is due to the inhomogeneous sound speed and density gradient induced by such a temperature distribution.

Such temperature variations occur in the exhaust systems of vehicles [13] where the bottom portion of the waveguide is in direct contact with the ambient atmosphere while the upper portion is either near or in contact with the body of the vehicle which is, of course, at a different temperature. As we shall show by our subsequent numerical analysis, such an induced temperature variation across the waveguide can significantly alter the modal characteristics of the exhaust system with a consequent modification in its overall effectiveness at suppressing selected acoustic frequencies.

In ocean acoustics [14], both depth and range dependent sound speeds are typically considered. Density gradients are usually ignored since the spatial scale of such variations is much larger than the wavelength of the acoustic disturbance. The same situation obtains in atmospheric propagation [15]. Unlike such ocean and atmospheric waveguides, the ducts under consideration in this paper are fully enclosed and hence density gradients *must* be accounted for.

For small perturbations of an isothermal ambient state, such an analysis was performed in [1, 2]. In [3], a numerical procedure was outlined for the case of arbitrary temperature distribution within the cross-section of the waveguide. Full details of the analysis and approximations as well as a supporting numerical example are provided in this paper.

The present study will commence with the formulation of a physical model which includes both an inhomogeneous sound speed and a density gradient across the duct. Uniform axial flow is also accomodated. The corresponding mathematical model will involve a generalized Helmholtz operator whose eigenvalues (related to the cut-off frequencies) and eigenfunctions (modal shapes) are to be determined. This continuous problem is discretized via the Control Region Approximation [7, 8, 9] (a finite difference procedure applicable to general geometries) resulting in a generalized matrix eigenvalue problem.

The aforementioned generalized eigenvalues and eigenvectors are then approximated numerically. In turn, this permits the determination of the cut-off frequency, dispersion curve and pressure distribution for each of the modes. This procedure is illustrated for the case of a rectangular duct with a heated wall. All numerical computations were performed using MATLAB©.

2 Physical Model

With reference to Figure 1, we consider the acoustic pressure field within an infinitely long, hard-walled, cylindrical duct of general cross-section, $\mathcal{W}$. The analysis of the modal propagation characteristics of such an acoustic waveguide typically proceeds by assuming a constant temperature throughout the undisturbed fluid.

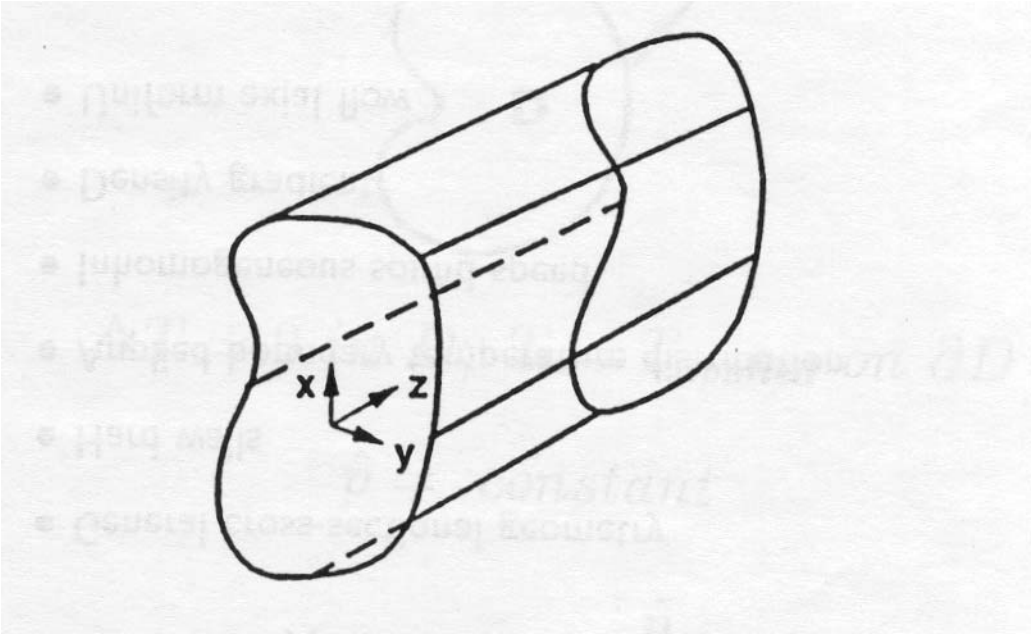

Figure 1: Acoustic Waveguide Cross-Section

However, in the present study, we permit a steady-state temperature variation throughout the waveguide cross-section (Figure 2). This temperature variation is due to an applied temperature distribution along the walls of the duct governed by the boundary value problem

$$\Delta T = 0 \; in \; \mathcal{W}; \; T = T_{applied} \; on \; \partial\mathcal{W} \tag{1}$$

where, here as well as in the ensuing analysis, all differential operators are transverse to the longitudinal axis of the waveguide.

This temperature variation across the duct will produce inhomogeneities in the background fluid density

$$\hat{\rho}(x,y) = \frac{\hat{p}}{R \cdot T(x,y)} \tag{2}$$

and sound speed

$$c^2(x,y) = \gamma R \cdot T(x,y), \tag{3}$$

where γ is the ratio of specific heats, R is the universal gas constant and $\hat{p}$ is the ambient pressure (which is constant).

The self-consistent governing equations for the hard-walled acoustic pressure wave with frequency ω and propagation constant β, $e^{j(\omega t - \beta z)} \cdot p(x,y)$, are [4] ($n$ is the direction normal to the waveguide wall):

$$\hat{\rho}\nabla \cdot (\frac{1}{\hat{\rho}}\nabla p) - \left[\nabla \cdot (\frac{1}{\hat{\rho}}\nabla\hat{\rho})\right] p + (\frac{\omega^2}{c^2} - \beta^2)p = 0 \; in \; \mathcal{W}; \; \frac{\partial p}{\partial n} = 0 \; on \; \partial\mathcal{W}, \tag{4}$$

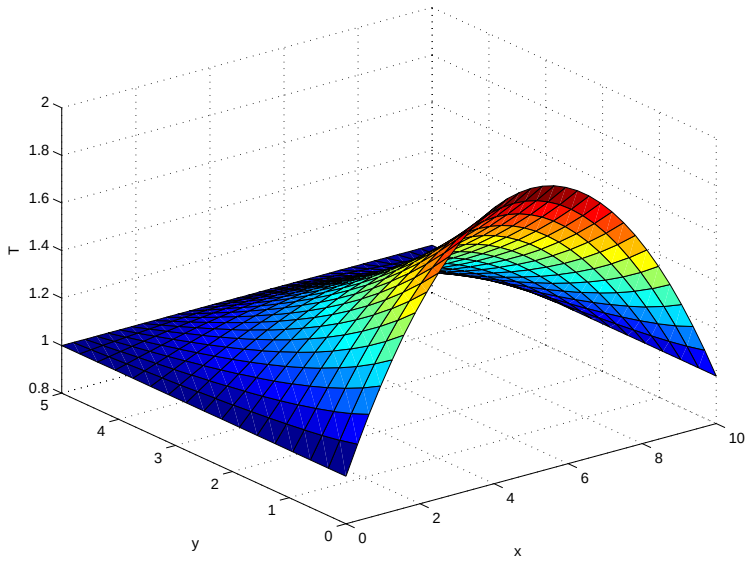

Figure 2: Temperature Profile

assuming that the fluid is at rest (the cut-off frequencies, corresponding to $\beta = 0$, are unaltered by uniform flow down the duct [5]).

However, a uniform axial flow with velocity V will alter the dispersion curves for the waveguide modes. In this event, the DeSanto model, Equation (4) may be modified as follows [5]:

$$\hat{\rho}\nabla\cdot(\frac{1}{\hat{\rho}}\nabla p) - \left[\nabla\cdot(\frac{1}{\hat{\rho}}\nabla\hat{\rho})\right]p + \left[\frac{(\omega - V\cdot\beta)^2}{c^2} - \beta^2\right]p = 0 \ in \ \mathcal{W}. \tag{5}$$

We next nondimensionalize the temperature so that the minimum scaled temperature is unity:

$$t(x,y) := \frac{T(x,y)}{T_{min}} \Rightarrow \hat{\rho}(x,y) = \frac{\rho_{max}}{t(x,y)}, \ c^2(x,y) = c^2_{min}\cdot t(x,y). \tag{6}$$

We then utilize Equation (6) to eliminate the density from Equation (5) which results in the generalized Helmholtz boundary value problem for $p(x,y)$:

$$\nabla\cdot(t\nabla p) - t\left[\nabla\cdot\left(t\nabla\left(\frac{1}{t}\right)\right)\right]p - \beta^2 tp = -\Omega^2 p \ in \ \mathcal{W}; \ \frac{\partial p}{\partial n} = 0 \ on \ \partial\mathcal{W}, \tag{7}$$

where

$$\Omega^2 := \left(\frac{\omega}{c_{min}} - M_{max}\cdot\beta\right)^2; \ M_{max} := \frac{V}{c_{min}}. \tag{8}$$

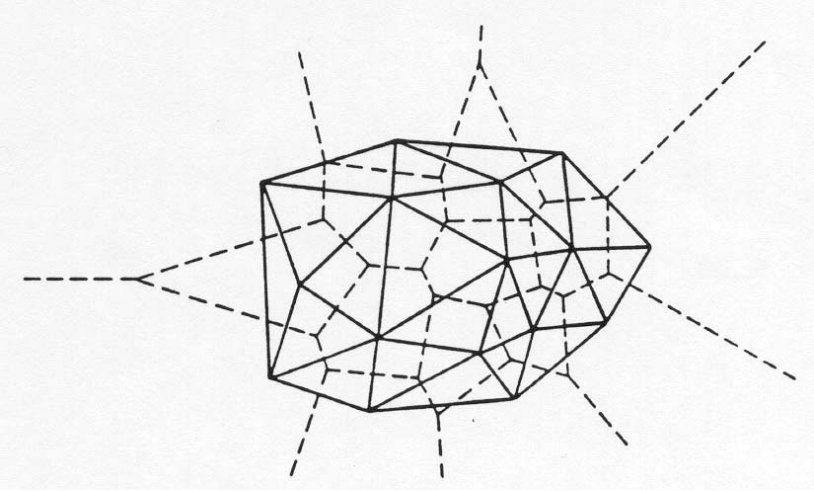

Figure 3: Dirichlet/Delaunay Tessellations

3 Control Region Approximation

The Control Region Approximation [7, 8] is a generalized finite difference procedure that accomodates arbitrary geometries [9]. It involves discretization of conservation form expressions on Dirichlet/Delaunay tessellations (see below). This permits a straightforward application of relevant boundary conditions.

The first stage in the Control Region Approximation is the tessellation of the solution domain by Dirichlet regions associated with a pre-defined yet arbitrary distribution of grid points. Denoting a generic grid point by P_i, we define its Dirichlet region as

$$D_i := \{P \ : \ ||P - P_i|| < ||P - P_j||, \ \forall j \neq i\}. \tag{9}$$

This is seen to be the convex polygon formed by the intersection of the half-spaces defined by the perpendicular bisectors of the straight line segments connecting P_i to P_j, $\forall j \neq i$. It is the natural control region to associate with P_i since it contains those and only those points which are closer to P_i than to any other grid point P_j.

If we construct the Dirichlet region surrounding each of the grid points, we obtain the Dirichlet tessellation of the plane which is shown dashed in Figure 3. There we have also connected by solid lines neighboring grid points which share an edge of their respective Dirichlet regions. This construction tessellates the convex hull of the grid points by so-called Delaunay triangles. The union of these triangles is referred to as the Delaunay tessellation. The grid point distribution is tailored so that the Delaunay triangle edges conform to $\partial\mathcal{W}$. It is essential to note that these two tessellations are dual to one another in the sense that corresponding edges of each are orthogonal.

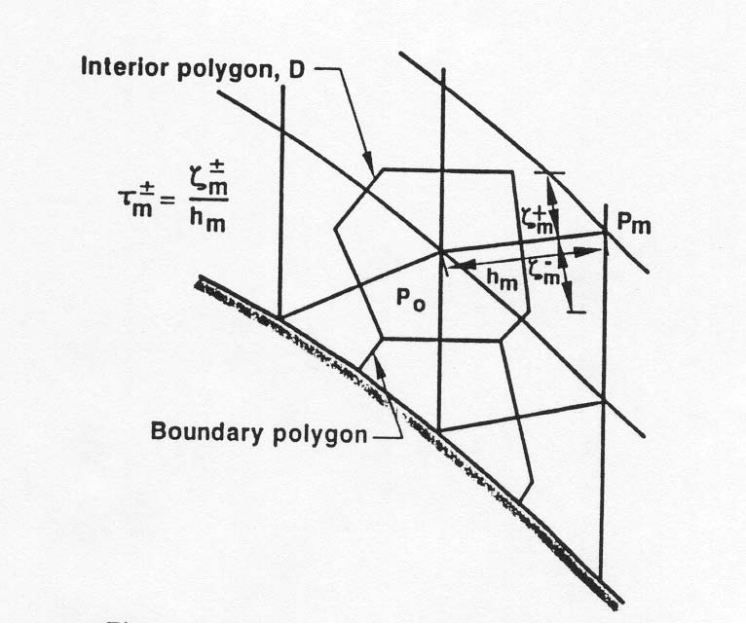

Figure 4: Control Region Approximation

With reference to Figure 4, we will exploit this duality in order to approximate the Dirichlet problem, Equation (1), for the temperature distribution at the point P_0. We first reformulate the problem by integrating over the control region, D, and applying the divergence theorem, resulting in:

$$\oint_{\partial D} \frac{\partial T}{\partial \nu}\, d\sigma = 0, \tag{10}$$

where (ν, σ) are normal and tangential coordinates, respectively, around the periphery of D. The normal temperature flux, $\frac{\partial T}{\partial \nu}$, may now be approximated by straightforward central differences [16] thereby yielding the Control Region Approximation:

$$\sum_m \tau_m\, (T_m - T_0) = 0, \tag{11}$$

where the index m ranges over the sides of D and $\tau_m := \tau_m^- + \tau_m^+$. Equation (11) for each interior grid point may be assembled in a (sparse) matrix equation which can then be solved for $T(x, y)$ (with specified boundary values) and *ipso facto* for $t(x, y)$.

It remains to discretize the homogeneous Neumann boundary value problem, Equation (7), for the acoustic pressure wave by the Control Region Approximation. For this purpose we first rewrite it in the integral form:

$$\oint_{\partial D} t \frac{\partial p}{\partial \nu}\, d\sigma - \int\int_D t \left[\nabla \cdot \left(t \nabla \left(\frac{1}{t}\right)\right)\right] p\, dA - \beta^2 \int\int_D tp\, dA = -\Omega^2 \int\int_D p\, dA. \tag{12}$$

We then approximate each of the integral operators appearing in Equation (12) as follows:

$$\oint_{\partial D} t\frac{\partial p}{\partial \nu}\, d\sigma \approx \sum_m\ \tau_m\ \frac{t_0+t_m}{2}\ (p_m - p_0), \tag{13}$$

$$-\int\int_D t\left[\nabla\cdot\left(t\nabla\left(\frac{1}{t}\right)\right)\right] p\ dA \approx -\left[\sum_m\ \tau_m\ \frac{(t_m-t_0)^2}{2t_m}\right]\cdot p_0, \tag{14}$$

$$-\beta^2\int\int_D tp\ dA \approx -\beta^2 t_0 A_0\cdot p_0, \tag{15}$$

$$\int\int_D p\ dA \approx A_0\cdot p_0, \tag{16}$$

where A_0 is the area of D (restricted to $\mathcal{W}$, if necessary) and we have utilized in Equation (14) the fact that $\sum_m \tau_m\ (t_m - t_0) = 0$ implies that

$$t_0\sum_m\ \tau_m\ \frac{t_0+t_m}{2}\cdot\left(\frac{1}{t_m}-\frac{1}{t_0}\right) = \sum_m\ \tau_m\ \frac{(t_m-t_0)^2}{2t_m}. \tag{17}$$

The hard boundary condition, $\frac{\partial p}{\partial \nu} = 0$, is enforced by simply modifying any τ_m in Equation (13) corresponding to boundary edges. Because $\Delta t = 0$, the approximation of Equation (14) remains valid for boundary points provided that the summation excludes the portion of ∂D lying on $\partial\mathcal{W}$.

4 Generalized Eigenvalue Problem

Substitution of Equations (13-16) into Equation (12) yields the matrix generalized eigenvalue problem [10]

$$Ap = \lambda Bp, \tag{18}$$

with $\lambda = -\Omega^2$ and where A is sparse and symmetric while B is positive and diagonal (its elements are precisely the areas of the Dirichlet polygons restricted to W). The reality of Ω is guaranteed by the following result.

Theorem 1 *The matrix A appearing in Equation (18) is nonpositive semidefinite.*

Proof: As A is comprised of the discrete operators of Equations (13-15), we consider separately the effect of each component upon the spectrum of A. By Gershgorin's Circle Theorem [17], the matrix corresponding to Equation (13) is nonpositive semidefinite (since the τ_m are nonnegative). By the Discrete Maximum Principle [18], t is positive throughout $\mathcal{W}$ so long as it is so along $\partial\mathcal{W}$ (which we have implicitly assumed throughout). Thus, adding the nonpositive

diagonal matrices corresponding to Equations (14) and (15) only serves to push the spectrum further to the left. Thus, A is seen to be nonpositive semidefinite. □

In computing the generalized eigenvalues of Equation (18), λ, we benefit greatly from the sparsity of A and the diagonality of B [11]. We may efficiently sweep out the modal dispersion curves by the following numerical procedure. Fix $\beta \geq 0$ and find $\Omega = \sqrt{-\lambda}$ from Equation (18). Then, obtain

$$\frac{\omega}{c_{min}} = \Omega + M_{max} \cdot \beta \tag{19}$$

from Equation (8) which may then be plotted versus β for any desired mode.

5 Numerical Example

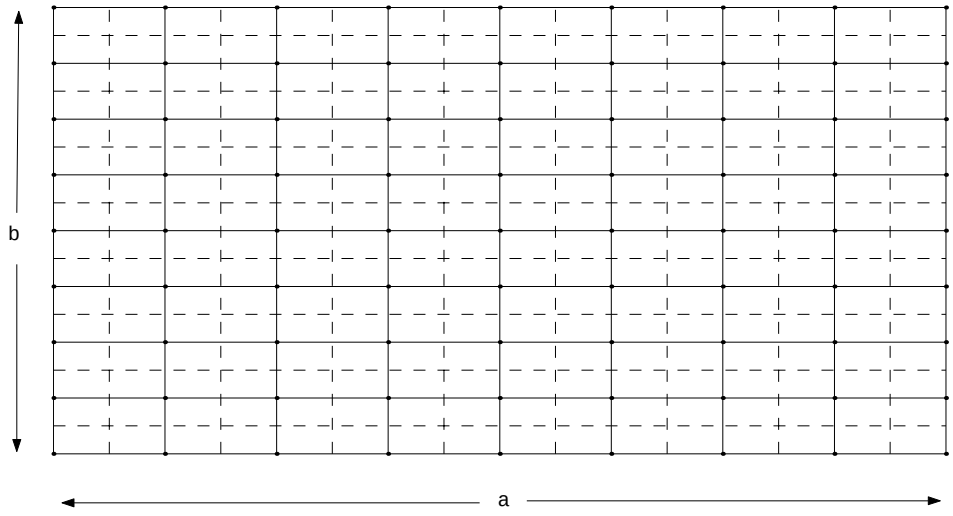

Figure 5: Rectangular Waveguide Cross-Section

With reference to Figure 5, we next apply the above numerical procedure to an analysis of the modal characteristics of the warmed rectangular duct with cross-section $\mathcal{W} = [0, a] \times [0, b]$. The exact eigenvalue corresponding to the (p, q)-mode with constant temperature is [12]:

$$\Omega_{p,q}^2 = \beta^2 + \left(\frac{p\pi}{a}\right)^2 + \left(\frac{q\pi}{b}\right)^2. \tag{20}$$

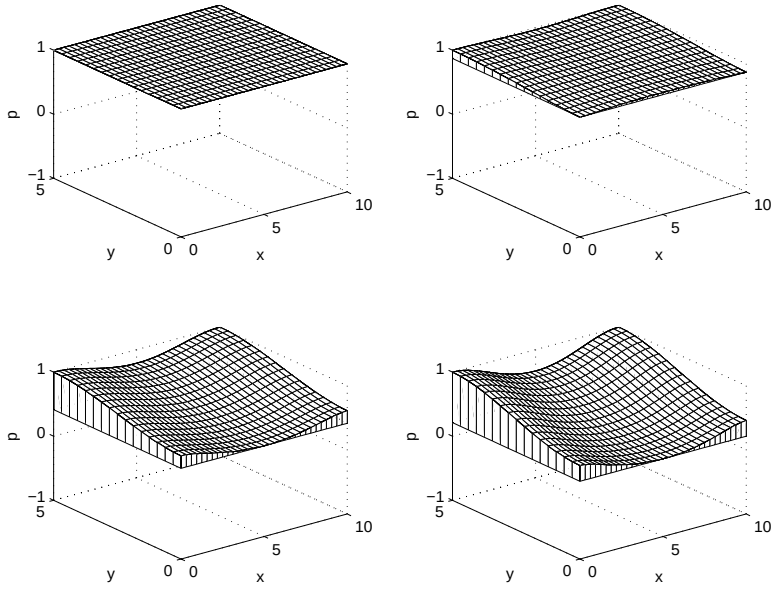

Figure 6: $(0, 0)$-Mode (Hard Wall)

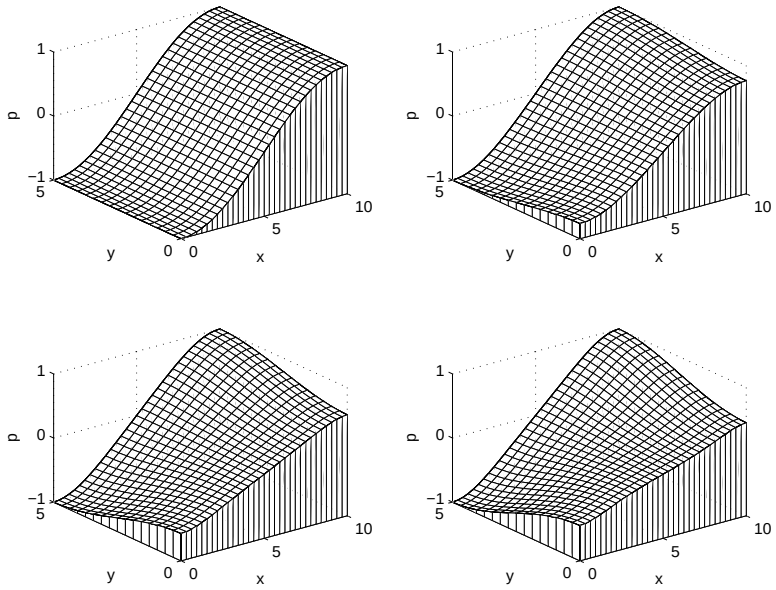

Figure 7: $(1, 0)$-Mode (Hard Wall)

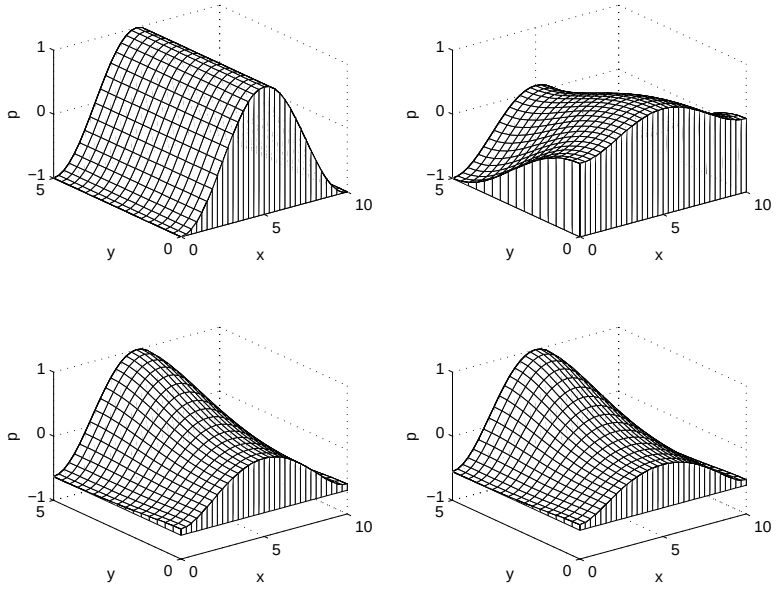

Figure 8: $(2,0)$-Mode (Hard Wall)

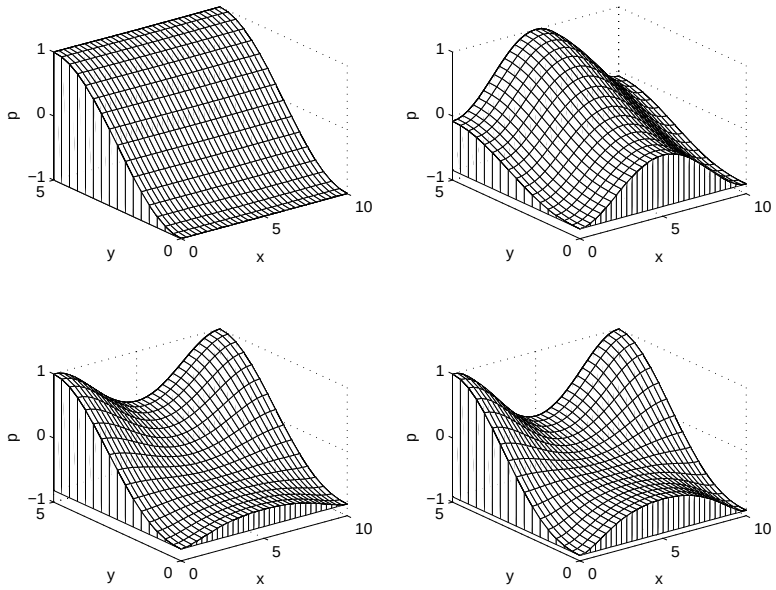

Figure 9: $(0,1)$-Mode (Hard Wall)

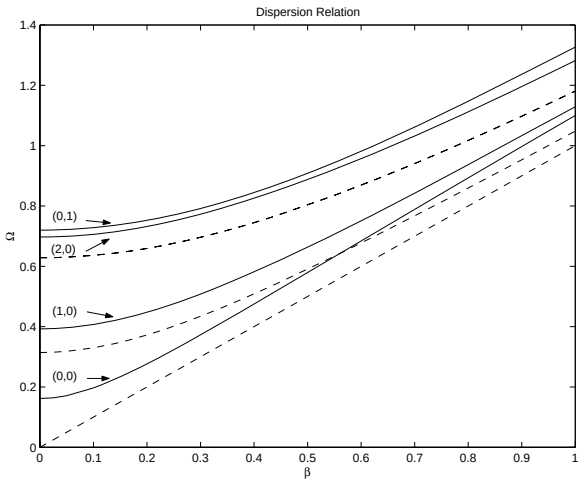

Figure 10: Spectral Structure (Warm Rectangular Waveguide)

For this geometry and mesh, the Dirichlet regions are rectangles and the Control Region Approximation reduces to the familiar central difference approximation [19]. Also, exact expressions are available for the eigenvalues and eigenvectors of the discrete operator in the constant temperature case [20].

The lower wall is subjected to the parabolic temperature profile

$$T_{applied} = 1 + \frac{4(T_{max} - 1)}{a^2} \cdot x(a - x). \tag{21}$$

while the other three walls are set to $T_{applied} = 1$. We then solve $\Delta T = 0$ by the procedure described above subject to this boundary condition for the cross-sectional temperature profile, $T(x, y)$, which is displayed in Figure 2.

Specifically, we set $a = 10$, $b = 5$, $T_{max} = 2$ and $V = 0$ so that $\Omega = \omega/c_{min}$. Utilizing 33×17 and 17×9 computational meshes followed by Richardson extrapolation [16], we display the first four computed modes (corresponding to the four smallest generalized eigenvalues) in Figures (6-9). In each figure, the plot in the upper left corresponds to constant temperature, $T = 1$, while that in the upper right corresponds to variable temperature with $\beta = 0$. The plots in the lower left/right correspond to variable temperature with $\beta = 0.5$ / 1.0, respectively. Figure 10 presents the dispersion relation corresponding to each of these four modes. The dashed curves correspond to constant temperature while the solid curves correspond to variable temperature. Of course, the cut-off frequency for each mode corresponds to $\beta = 0$.

Collectively, these figures tell an intriguing tale. Firstly, the $(0, 0)$-mode is no longer a plane wave in the presence of temperature variation. In addition, all variable-temperature modes possess a cut-off frequency so that, unlike the case of constant temperature, the duct cannot support any propagating modes at

the lowest frequencies. Moreover, the presence of a temperature gradient alters all of the cut-off frequencies. In sharp contrast to the constant temperature case, the variable-temperature modal shapes are frequency dependent. Lastly, the presence of a temperature gradient removes the modal degeneracy between the $(2,0)$- and $(0,1)$-modes that is prominent for constant temperature.

6 Conclusion

The preceding sections have presented a physical model as well as a numerical procedure for studying the modal characteristics of cylindrical acoustic waveguides in the presence of temperature gradients induced by an applied temperature distribution along the walls of the duct. Rather than simply making the sound speed spatially varying, as is done in atmospheric propagation and underwater acoustics, we have been careful to utilize a self-consistent physical model (due to DeSanto [4]) which also includes density gradients since we have dealt here with a fluid fully confined to a narrow region. Also, we have extended DeSanto's model to allow for uniform axial flow down the duct.

While previous work [1, 2] was restricted to small perturbations of a constant temperature profile, the present paper allows arbitrary cross-sectional temperature profiles. Moreover, the Control Region Approximation developed herein permits waveguide cross-sections of arbitrary shape. We have presented a detailed numerical example (utilizing MATLAB©) intended to intimate the broad possibilities offered by the resulting numerically computed cut-off frequencies, dispersion curves and modal shapes.

7 Acknowledgement

I would like to thank my devoted wife Mrs. Barbara A. McCartin for her indispensable aid in constructing the figures.

References

[1] B. J. McCartin, A Perturbation Method for the Modes of Cylindrical Acoustic Waveguides in the Presence of Temperature Gradients, *Journal of Acoustical Society of America*, 102 (1) (1997), 160-163.

[2] B. J. McCartin, Erratum, *Journal of Acoustical Society of America*, 113 (5) (2003), 2939-2940.

[3] B. J. McCartin, A Numerical Procedure for 2D Acoustic Waveguides with Heated Walls, *Bulletin of American Physical Society*, 44 (3) (1999), 38.

[4] J. A. DeSanto, *Scalar Wave Theory*, Springer-Verlag, Berlin, 1992.

[5] P. M. Morse and K. U. Ingard, Linear Acoustic Theory, *Handbuch der Physik, Vol. XI/1, Acoustics I*, S. Flügge (ed.), Springer-Verlag, Berlin, 1961, 1-128.

[6] D. S. Jones, *Acoustic and Electromagnetic Waves*, Oxford, 1986.

[7] B. J. McCartin, Numerical Computation of Guided Electromagnetic Waves, *Proceedings of the 12th Annual Conference on Applied Mathematics*, U. Central Oklahoma, Edmond, OK, 1996, 127-140.

[8] B. J. McCartin, Control Region Approximation for Electromagnetic Scattering Computations, *Computational Wave Propagation*, B. Engquist and G. A. Kriegsmann (eds.), Springer-Verlag, New York, 1996, 141-164.

[9] B. J. McCartin, Seven Deadly Sins of Numerical Computation, *American Mathematical Monthly*, 105 (10) (1998), 929-941.

[10] J. H. Wilkinson, *The Algebraic Eigenvalue Problem*, Oxford, 1965.

[11] Y. Saad, *Numerical Methods for Large Eigenvalue Problems*, Halsted, New York, 1992.

[12] H. R. L. Lamont, *Waveguides*, Third Edition, Methuen, London, 1950.

[13] M. L. Munjal, *Acoustics of Ducts and Mufflers*, Wiley, New York, 1987.

[14] L. M. Brekhovskikh and Yu. P. Lyasov, *Fundamentals of Ocean Acoustics*, Second Edition, Springer-Verlag, Berlin, 1991.

[15] L. Brekhovskikh and V. Goncharov, *Mechanics of Continua and Wave Dynamics*, Springer-Verlag, Berlin, 1985.

[16] S. D. Conte and C. de Boor, *Elementary Numerical Analysis: An Algorithmic Approach*, Third Edition, McGraw-Hill, New York, 1980.

[17] D. S. Bernstein, *Matrix Mathematics*, Princeton University Press, Princeton, 2005.

[18] K. W. Morton and D. F. Myers, *Numerical Solution of Partial Differential Equations*, Second Edition, Cambridge University Press, Cambridge, 2005.

[19] A. Thom and C. J. Apelt, *Field Computations in Engineering & Physics*, Van Nostrand, London, 1961.

[20] F. B. Hildebrand, *Finite-Difference Equations and Simulations*, Prentice-Hall, Englewood Cliffs, NJ, 1968.

Received: October, 2008